



OPEN Design and motion analysis of a coal mine robot with variable wheel diameter

Liguo Han^{1,2}, Fei Ding^{1,2}✉, Lijuan Zhao³, Peng Li^{1,2}, Chuanzong Li^{1,2}, Mingjun Liu^{1,2}, Liangliang Ren¹ & Yuhao Li¹

In response to the complex unstructured environment of coal mines, a design scheme for variable wheel diameter robots is proposed. Based on the gear, connecting rod and sliding rail mechanism, a wheel with variable diameter was designed. Through the change in the wheel diameter of the robot, the obstacle-crossing ability and terrain adaptation ability of the robot were improved. The kinematic model of a single wheel was established and the variation rule of radial length was analysed. The kinematics model of the whole vehicle was established, and the motion state of the robot under different driving speeds was analysed. Based on RecurDyn software, the robot turning, wheel diameter change process and obstacle surmounting process were simulated. Through 3D printing technology, the robot prototype was made, and the limit obstacle crossing test was carried out. Simulations and prototype tests show that the smallest radius of the wheel radius change is 107 mm, the largest radius is 158 mm, and the limit height for the robot to cross obstacles is 172 mm. After the wheels are unfolded, the centroid of the robot rises by 50 mm, and the fluctuation amplitude of the centroid of the robot when walking with the maximum radius is 3.6 mm. The diameter was increased by 47.6% through the gear, link and sliding rail mechanism, and the exceeding limit height was increased by 60.7% compared with the common wheel-type robot. Compared with tracked and legged robots, the robot designed in this article has high flexibility and lightweight. It can reduce the wheel diameter and accelerate forward on flat roads, and when encountering obstacles, it can increase the wheel diameter to improve obstacle crossing performance. This provides new ideas for the research of special detection robots and the intelligence of coal mines in the future.

Keywords Fossil energy, Intelligent coal mine, Coal mine robot, Wheel diameter variable robot, Kinematic analysis, Linkage mechanism

For the underground unstructured environment, it is an important research direction in the field of coal mine intelligence to develop robots that are practical and suitable for the underground complex working environment. It is of great significance to coal mine safety production and reduces the loss of life and property of the state and people¹⁻³. Coal mine disasters are usually accompanied by collapses and roof falls, and crushed coal and puddles make it more difficult for robots to walk⁴. Therefore, it is particularly urgent to carry out research on new robots with flexible movement and strong terrain adaptability.

The shape-shifting robot has good passing ability and is well suited for rescue detection tasks downhole. Compared with the track mechanism, the wheel drive mechanism is simple, stable and efficient, but its mobility in unstructured terrain is seriously limited. Using a variable wheel diameter hub is one of the methods to improve the mobility of wheel-driven robots⁵. Research has been performed on variable wheel diameter robots. Nagatani K et al.⁶ designed a rescue robot with variable wheel diameters for narrow and rugged environments and analysed and tested the obstacle climbing ability of the robot. Chenxb et al.⁷ A robot was designed to realize spoke deformation by the relative rotation between the hubs, and the dynamic simulation of the wheel was carried out to obtain the minimum torque required for the diameter change of the wheel. Je-sung Koh et al.^{8,9} designed a variable wheeled robot with three driving modes and made a prototype. Zhao x et al.¹⁰ designed a deformable wheel-leg robot that can switch between the two modes on the wheel legs and carried out simulation analysis. Guo Pengcheng¹¹ introduced a modified wheel adapted to complex road conditions and analysed the

¹School of Computer and Information Engineering, Fuyang Normal University, Fuyang 236037, China. ²Anhui Engineering Research Center for Intelligent Computing and Information Innovation, Fuyang Normal University, Fuyang 236037, China. ³School of Mechanical Engineering, Liaoning Technical University, Fuxin 123000, China. ✉email: dingfei01@126.com

mechanical characteristics before and after the change based on MATLAB software. Xie Xiaolin et al.¹² designed a variable wheel for soft ground and analysed the traction characteristics. Yang Yang et al.¹³ proposed four kinds of multisection variable wheel mechanisms by combining the wheel style, extended style and wheel-leg style configuration with a polygon mechanism. At the same time, the advantages and disadvantages of each configuration were compared and optimized for the better scheme. Cong Peichao et al.¹⁴ designed a deformable wheel mobile robot. With the help of the self-locking effect between the “push rod” and the “plane screw pair”, a lifting universal wheel mechanism was set, which effectively solved the “wheel piece retraction” of the deformable wheel and optimized the mechanism control of the system. Deng Zhiyan¹⁵ designed a denatured wheel with a large load and carried out processing and test verification. Chen Zhihua et al.^{16–18} proposed a parallel six wheeled mobile robot (bit-6naza), which is equipped with Stewart type leg structure and has large load capacity. It integrates the advantages of wheel and foot movements, and can realize foot, wheel and wheel foot compound movements. Through the control strategy of multi-sensor information feedback, the six legged robot can walk stably on unstructured terrain. Based on paper folding theory, the research group proposed a water spring wheel model with a parallelogram structure, which was applied in the field of coal mine rescue robots, and developed a prototype, which has the characteristics of high flexibility and strong obstacle surmounting ability^{19–22}. However, the paper folding structure is complex, the manufacturing is difficult, the production cost is huge, and it is difficult to apply in practice. In the face of the underground unstructured environment, the crease is easy to enter the sand and stone, and it is difficult to shrink and deform. Rubio Francisco²³ and others systematically reviewed the concept, method, theoretical framework and application of mobile machines. Zhang Aimin et al.²⁴ provided a design and application of inspection robot for coal mine fully mechanized working face, including rigid flexible integrated track, robot body, driving device, etc. the wire rope moves along the rigid flexible integrated track under the traction of the driving device, which can be widely used in the field of coal mine inspection. Wang Luming et al.²⁵ explained the development and research status of coal mine tunneling robot, coal mining robot and rescue robot, and looked forward to its development trend in view of the existing problems, providing a reference for the development of coal mine robot technology. Song Rui et al.²⁶ summarized the research status of key technologies such as bionic mechanism, bionic perception, bionic control, bionic drive and bionic materials, and expounded the advantages and applicable scenarios of bionic technology compared with existing equipment, and looked forward to the application prospects of bionic robot technology in unmanned operation of coal mines: the application of new functional materials, the application of efficient walking mode, the application of intelligent environmental perception, the application of intelligent autonomous operation. It provides reference for the development and utilization of bionic robot in coal mine. Zhang Feng²⁷ in order to improve the service life of the pipeline and prevent the aging, corrosion and fracture of the pipeline, a variable diameter pipeline inspection robot was designed, and its motion simulation was carried out to verify the feasibility of pipeline inspection. The robots studied above can be broadly divided into three categories: (1) A robot with complicated mechanical structure and wheel leg transformation; (2) Soft deformation robot with material and structure characteristics; (3) A robot that works in a specific place underground. These three types of robots have the following disadvantages: (1) Wheeled legged robot with complex mechanical structure has strong load capacity, but it is difficult to apply in small space due to its large size. (2) The soft robot is very suitable for small space. In the underground environment, the reliability is low due to the soft structure. (3) The robots working in specific underground places have some structures fixed in the underground, so they have poor flexibility and mobility. The complexity of the actual underground environment and the lack of grasp of the actual situation after the disaster make it difficult to fully consider the characteristics of roadblocks, dangerous gases, dust, ponding and other characteristics of the detected mine in the design and development of the coal mine robot, thus directly or indirectly affecting the reliability of the robot^{28,29}. The complex and changeable unstructured task environment in the mine puts forward higher and higher requirements for the practicability of robots. Designing and developing robots with simple structure, low production cost and high reliability is still a technical problem to realize the intellectualization of coal mines.

In this paper, a new design scheme of variable wheel diameter robot is proposed. The robot keeps the minimum diameter and walks in the form of round wheels in smooth road conditions. When encountering obstacles, the wheel diameter increases and the gap between adjacent spokes can easily cross the obstacles. The diameter of the wheel is changed by a simple gear slide mechanism, and the gear is selected with appropriate standard parts. The production cost is extremely low, and the simple structure improves the reliability. Through mathematical analysis, the number of slideway groups of the variable diameter wheel is determined, and the whole robot model is designed with Creo software. The kinematics model of the robot is constructed. Based on the virtual prototype technology, the simulation of the robot's turning in situ, wheel diameter changing process and obstacle crossing limit is carried out. Finally, the machine prototype is made by 3D printing technology. The maximum obstacle crossing height is determined by obstacle crossing test, and the feasibility and correctness of the design scheme are verified.

Structural design of the variable diameter wheel

Determination of the number of variable diameter wheel slideway groups

The obstacle surmounting the performance of a wheeled robot is related to the wheel diameter. With increasing wheel diameter, the obstacle surmounting performance is stronger. The robot can improve the obstacle surmounting performance by changing the wheel diameter when surmounting obstacles. When the robot crosses the obstacle, the rim gap between the two adjacent groups of slides will be stuck on the obstacle, increasing the grip and improving the ability to cross the obstacle. Therefore, the number of slide groups has a great influence on the obstacle-crossing performance of the rescue robot and the driving force of the motor. The maximum obstacle-crossing height and the maximum driving force required for obstacle-crossing can be determined by Eqs. (1)–(4)^{30–32}:

$$h_i = r (\sin (\pi / i) + \cos \alpha_i) \quad (1)$$

where i is the number of slide groups, r is the wheel radius and α_i is the angle between the vertical line from the centre of the wheel to the ground and the nearest connecting rod.

$$F_a - N_1 \sin \beta_i + F_1 \cos \beta_i = 0 \quad (2)$$

$$F_1 \sin \beta_i + N_1 \sin \beta_i - G = 0 \quad (3)$$

$$T - N_1 R = 0 \quad (4)$$

Where $F_1 = \mu \cdot N_1$ and F_a is the driving force required for obstacle crossing, β_i is the angle between the slide rail in contact with the step and the horizontal direction, G is the gravity of the body acting on the wheel and the gravity of the wheel itself, μ is the friction coefficient between the wheel and the supporting surface, T is the driving torque, and N_1 is the supporting force from the supporting face to the wheel.

The following can be obtained by solving the joint Eqs. (2)–(4):

$$F_a = \frac{1 - \mu \cot \beta_i}{\mu + \cot \beta_i} G \quad (5)$$

The calculation results of Eqs. (1) and (5) are sorted out, as shown in Table 1.

It can be seen from Table 1 that when the number of slide rail groups is 2, 3 and 5, the wheel's obstacle surmounting ability is better, and when the number of slide rails is 2, 3, 4 and 5, the driving force decreases significantly. The analysis was carried out with the obstacle surmounting performance as the main and the driving force as the supplement, the number of deformed wheel and rail groups is finally determined to be 5.

Structure and complete machine design of the variable diameter wheel

The structure of the variable diameter wheel is shown in Fig. 1. The wheel diameter can be adjusted according to the changes in road surface and environmental conditions. The motor transmits the power to the rocker through the gear set, and the connecting rod drives the umbrella rim to move in the hub chute to realize the real-time change in wheel diameter. The overall structure and 3D solid model of the robot are shown in Fig. 2. The overall structure consists of a reducer, drive shaft, vertical bearing seat, motor frame, girder and shell. The girder is designed as an upper convex structure, which improves the obstacle crossing height and does not easily touch the bottom. Each drive shaft is installed on two vertical bearing seats to prevent the dislocation of the axle when the robot changes the direction of motion. The steel bar erecting mechanism is set at the bottom of the girder and chassis to ensure the high load capacity of the robot.

Kinematic model construction headings

Kinematic analysis of wheels

The variable diameter wheel folding motion is achieved through gears, connecting rods, and sliding rails. The overall model of the wheel is shown in Fig. 3. Assuming that the deformation motor moves at an angular velocity ω_p , the length of the rocker arm is a , the length of the connecting rod is b , the initial angle of the rocker arm is θ , and the change in wheel diameter Δ after time t can be determined by Eqs. (6)–(8).

As shown in the Fig. 3, the joystick, connecting rod, and sliding rail enclose a triangle. Assuming the initial length of the inclined edge (sliding rail) is c , the length of the inclined edge (sliding rail) after deformation operation is d . Based on the characteristics of triangles and the cosine theorem, it can be concluded that:

$$c^2 = b^2 - a^2 + 2 \cdot a \cdot c \cdot \cos \theta \quad (6)$$

$$d^2 = b^2 - a^2 + 2 \cdot a \cdot d \cdot \cos(\theta - \omega_p t) \quad (7)$$

$$\Delta = 2(d - c) \quad (8)$$

i	Included angle between sliding rails (deg)	α_i (deg)	β_i (deg)	h_i	F_a ($\mu=0.1$)
2	180	0	90	2r	10G
3	120	30	60	1.732r	1.391G
4	90	45	45	1.414r	0.818G
5	72	18	36	1.539r	0.584G
6	60	0	30	1.5r	0.451G
8	45	5	22.5	1.38r	0.302G
12	18	0	9	1.259r	0.164G

Table 1. Influence of the number of slide rail groups on obstacle surmounting ability and driving force.

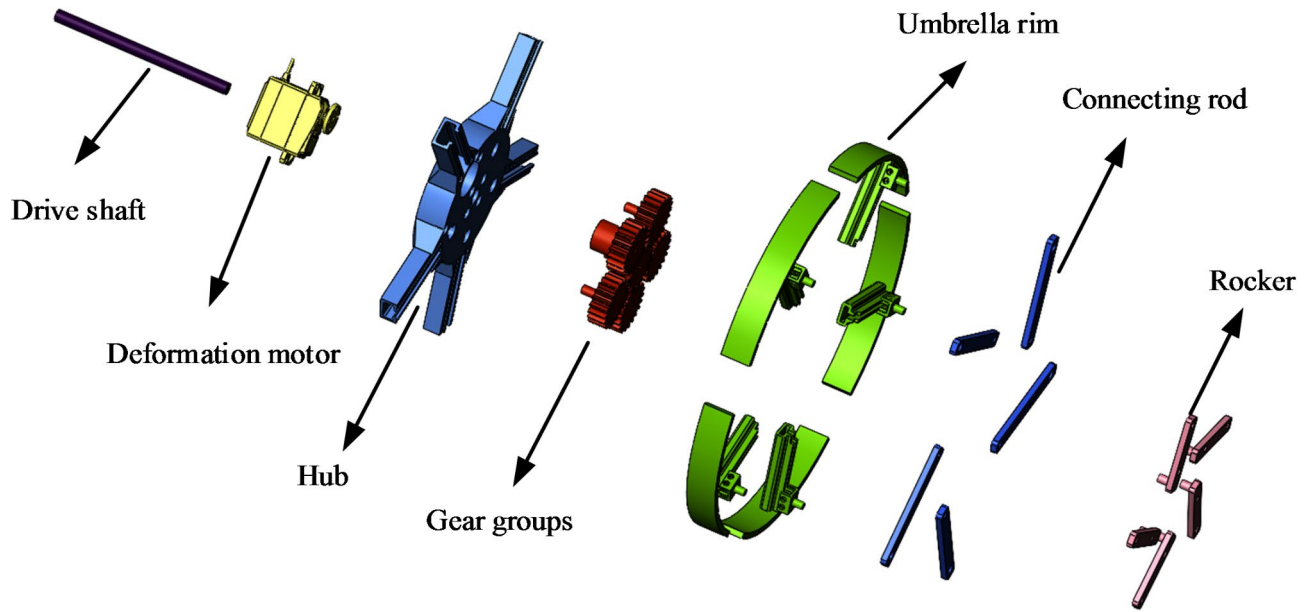


Fig. 1. Structure of the variable diameter wheel.

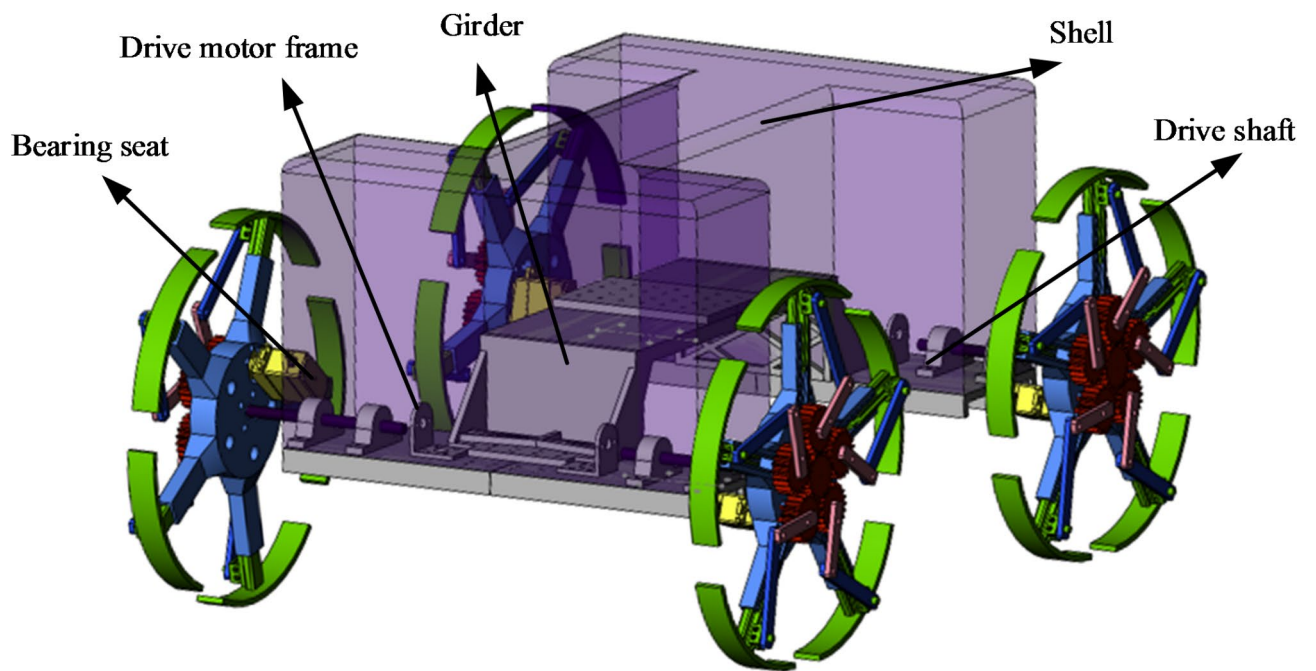


Fig. 2. 3D solid model of robot.

Kinematic modelling of robot

According to the structural characteristics of the robot with a variable wheel diameter, the kinematics model of the robot is established. The robot is assumed to be in contact with the ground and subject to friction in the process of motion. There is no slip phenomenon, and the centroid coincides with the center of shape. The four independent drive wheels are modelled at the minimum radius, as shown in Fig. 4. The symbols in Fig. 4 and Eqs. (9)–(15) are shown in Table 2.

For a variable diameter wheel

$$v_i = \omega_i r \tag{9}$$

From the speed of the robot body

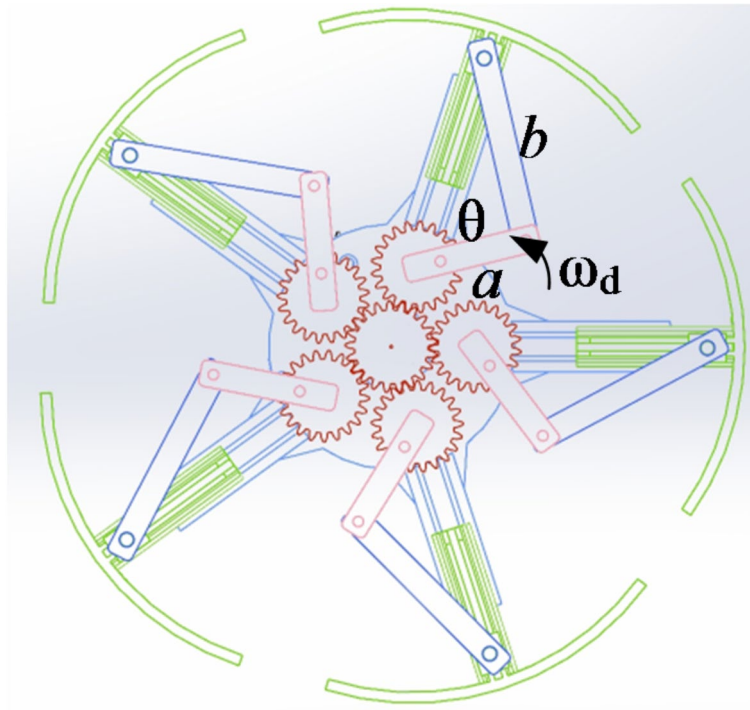


Fig. 3. Schematic diagram of the overall model of the wheel.

$$v_i = v_\eta \pm \omega_z D \sin \delta \tag{10}$$

From Eqs. (9)–(10):

$$\omega_i = \begin{bmatrix} \frac{1}{r} & 0 & \pm \frac{D \sin \delta}{r} \end{bmatrix} \begin{bmatrix} v_\zeta \\ v_\eta \\ \omega_z \end{bmatrix} \tag{11}$$

For variable diameter wheels 1–4:

$$v_{1,2} = (R + D \sin \delta) \omega_k \tag{12}$$

$$v_{3,4} = (R - D \sin \delta) \omega_k \tag{13}$$

From Eqs. (12)–(13):

$$R = \frac{\omega_{1,2} + \omega_{3,4}}{\omega_{1,2} - \omega_{3,4}} \cdot D \sin \delta \tag{14}$$

The relationship between the angular velocity of the variable diameter wheel drive and the motion state of the robot body and geodetic coordinate system can be obtained by coordinate transformation^{33,34} and Eq. (11):

$$\begin{bmatrix} \omega_1 \\ \omega_2 \\ \omega_3 \\ \omega_4 \end{bmatrix} = \begin{bmatrix} 1/r & 0 & D \sin \delta / r \\ 1/r & 0 & D \sin \delta / r \\ 1/r & 0 & -D \sin \delta / r \\ 1/r & 0 & -D \sin \delta / r \end{bmatrix} \begin{bmatrix} \cos \vartheta & \sin \vartheta & 0 \\ -\sin \vartheta & \cos \vartheta & 0 \\ 0 & 0 & 1 \end{bmatrix} \begin{bmatrix} \dot{p} \\ \dot{q} \\ \dot{\vartheta} \end{bmatrix} = \begin{bmatrix} \cos \vartheta / r & \sin \vartheta / r & D \sin \delta / r \\ \cos \vartheta / r & \sin \vartheta / r & D \sin \delta / r \\ \cos \vartheta / r & \sin \vartheta / r & -D \sin \delta / r \\ \cos \vartheta / r & \sin \vartheta / r & -D \sin \delta / r \end{bmatrix} \begin{bmatrix} \dot{p} \\ \dot{q} \\ \dot{\vartheta} \end{bmatrix} \tag{15}$$

Simulation test

To verify the rationality and feasibility of the design of the variable wheel diameter robot, the simulation test was carried out by RecurDyn v9r4 software. Robot parts established by Creo 8.0 software are imported into RecurDyn after assembly interference inspection to define part materials and add constraints and drives.

Turning simulation

According to Eq. (13), When the rotational speeds of the left and right wheels of the deformable wheel robot are not consistent, turning motion is performed through differential control. Set the driving function of wheel 1 and wheel 2 in RecurDyn software as $\text{step}(\text{time}, 0, 0, 1, -180\text{d}) + \text{step}(\text{time}, 11, 0, 12, 180\text{d})$. The drive function of wheel 3 and wheel 4 is $\text{step}(\text{time}, 0, 0, 1, 180\text{d}) + \text{step}(\text{time}, 11, 0, 12, -180\text{d})$. After the left and right wheel drive settings are completed, the simulation is carried out. The simulation time is set to 12 s. The robot centroid

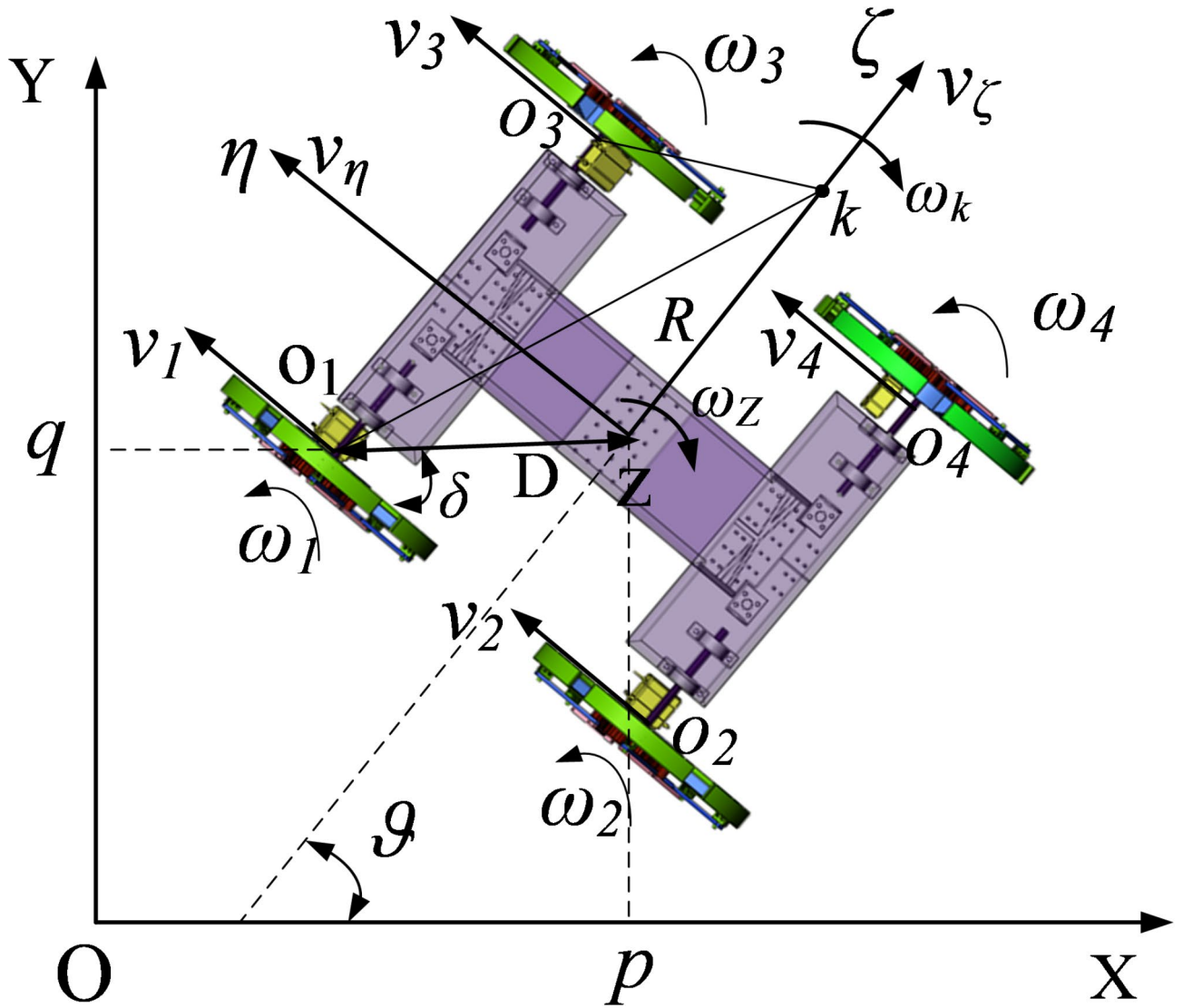


Fig. 4. Robot kinematics model.

Symbol	Meaning	Symbol	Meaning
XOY	Geodetic coordinate system	v_η	Robot η directional velocity
$\zeta z \eta$	Robot coordinate system	v_ζ	Robot ζ directional velocity
o_i	Driving wheel centre	ω_z	Robot z-point angular velocity
v_i	Drive wheel η directional velocity	p	Robot centre Z in geodetic coordinates
ω_i	Angular speed of driving wheel	q	Robot centre Z in geodetic coordinates
ϑ	Angle between coordinate systems	k	Robot rotation centre
D	Diagonal length of robot	δ	Diagonal angle
R	Turning radius	ω_k	Turning angular speed

Table 2. Symbol meaning.

wheel centre track and the displacement curve in the X- and Y-directions of the centroid are obtained by using the postprocessing module, as shown in Fig. 5.

Equation (13) shows that the robot can theoretically turn at zero radius in place at this time. From Fig. 5b, the fluctuation value of the robot centroid in the X-direction is -5.65 to 3.83 mm, the fluctuation displacement is 9.48 mm, the fluctuation value of the robot centroid in the Y-direction is -188.2 mm to -181.1 mm, and the fluctuation displacement is 7.1 mm, from this, it can be concluded that the average turning radius of the robot is 4.2 mm. These fluctuations can be ignored with respect to the overall size of the robot. Therefore, the fluctuations

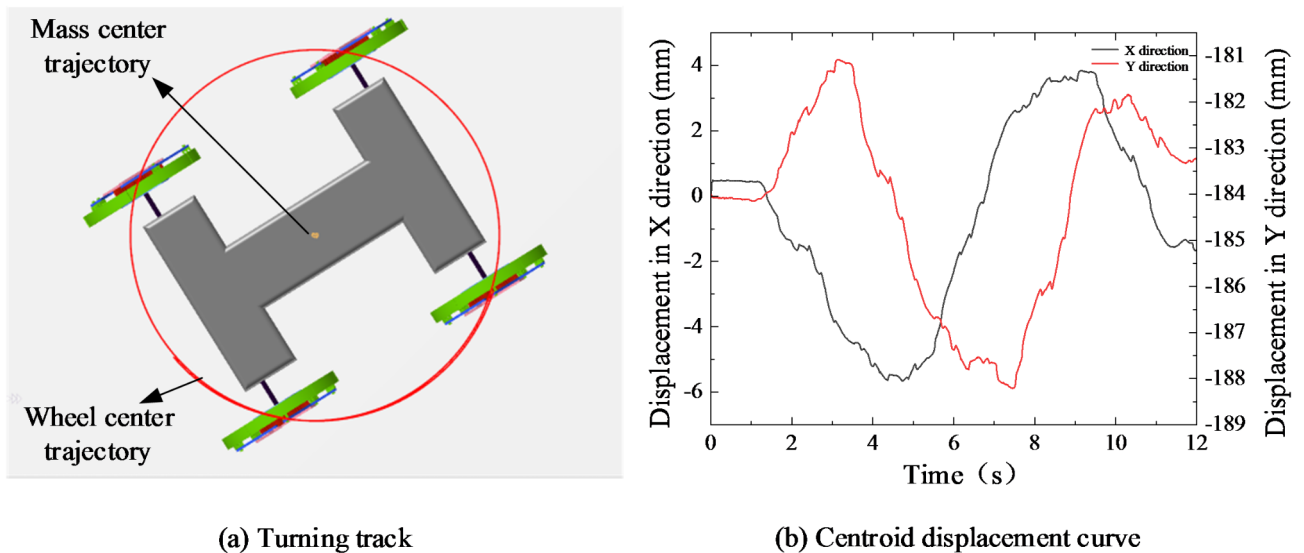


Fig. 5. Robot turning simulation.

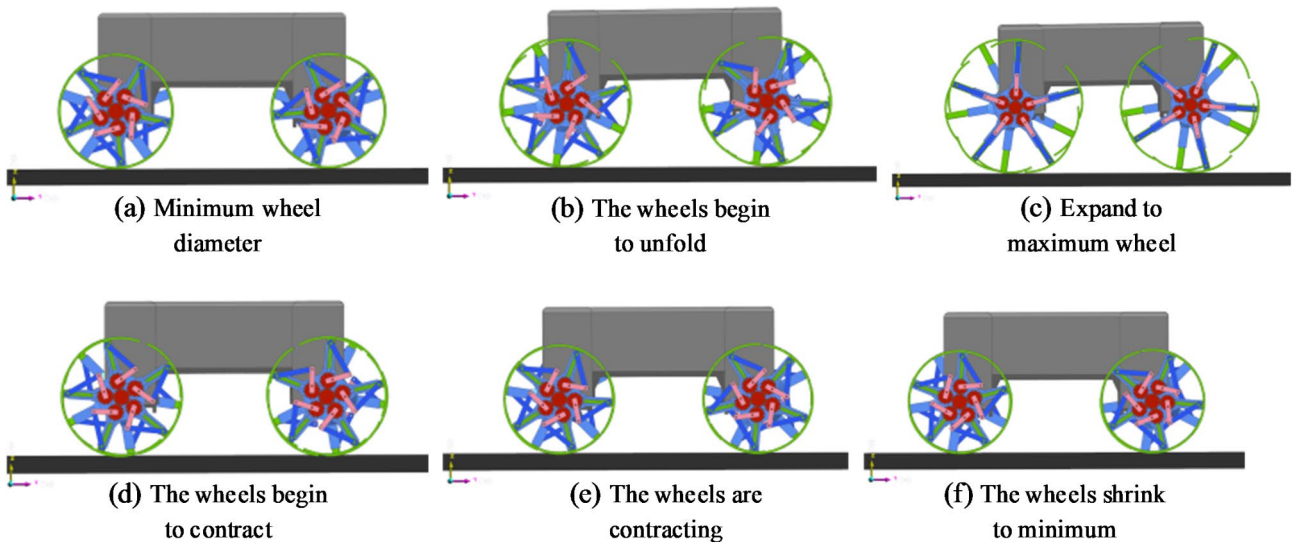


Fig. 6. Diagram of the deformation process.

can be regarded as having no displacement in the X- and Y-directions and realize zero radius rotation around the Z-direction. The correctness of the model and the rationality of the structural design are verified when the wheel radius is minimal.

Deformation simulation

Wheel diameter variable robot adjusts the wheel diameter reasonably according to the working terrain and environment through the gear, link and rail structure, so whether the wheel can be folded smoothly is very important to the performance of the robot. This section validates the folding process of the robot through simulation tests. Add a velocity type drive to the drive shaft with the drive function set to $\text{step}(\text{time}, 0, 0, 0.5, 0) + \text{step}(\text{time}, 0.5, 0, 1, -180\text{d}) + \text{step}(\text{time}, 13, 0, 13.5, 180\text{d})$, add a disp type drive to the gear connected to the deformation motor and set the drive function to $\text{step}(\text{time}, 3, 0, 5, -80\text{d}) + \text{step}(\text{time}, 9, 0, 11, 80\text{d})$, and the simulation time is 13.5 s. The sketch diagram of the deformation process of a wheel-diameter variable robot is shown in Fig. 6, the obtained centroid displacement diagram of the robot is shown in Fig. 7, and the change in driving torque during deformation is shown in Fig. 8. The attitude angle of the robot during deformation is shown in Fig. 9.

Figure 6 shows that the variable diameter wheel smoothly completes the transition from the minimum radius to the maximum radius and then back to the minimum radius. Figure 7 shows that during the course of the radius change of the deformation wheel from minimum to maximum, the centre of mass of the robot

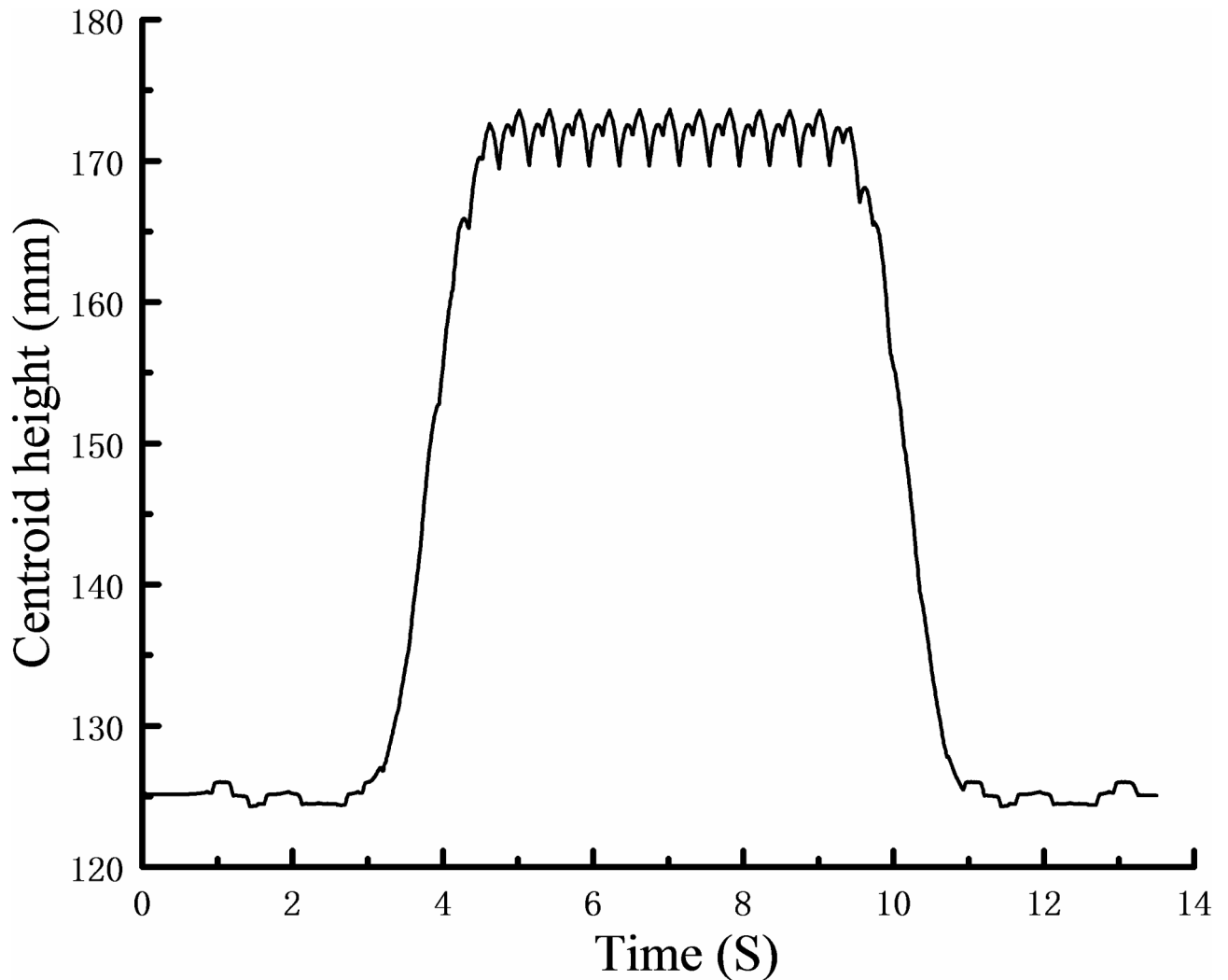


Fig. 7. Mass centre displacement curve during deformation.

increases by 50 mm, and the fluctuation range of the centre of mass is 3.6 mm when walking with the maximum radius, which shows periodic change. Figure 8 shows that the required driving torque under a small radius of the deformation wheel is less than 10 N m and under 30 N m at the maximum radius. These data provide a basis for motor selection when prototyping a robot. Figure 9 illustrates the posture change of the body of the robot during the deformation process. During the whole deformation process, the posture angle change amplitude is about 1 deg. The machine starts to deform after 3 s, and the pitch angle and roll angle fluctuate periodically. This is because there is a gap between the umbrella rim after the wheels are deployed. After the deployment, the four points are not coplanar when the four wheels contact the ground.

Simulation of obstacle crossing boundary

The underground terrain environment is complex and changeable and requires high obstacle surmounting performance. The robot simulates the process of the limit obstacle height to verify the feasibility of the overall design scheme. The simulation test takes the step as the target obstacle, continuously increasing the step height, and finally determines that the obstacle crossing limit height is 180 mm. A schematic diagram of the obstacle crossing process is shown in Fig. 10, and the parameter changes are shown in Fig. 11.

Figure 10 shows the complete process of the robot climbing steps after the transition from the minimum radius state to the maximum radius state, then from the maximum radius state to the minimum radius state on the steps, and finally stopping. Figures 10 and 11 show that within 0–3 s, the robot starts to move with the minimum radius, and the wheel angular speed increases from 0 to 270 d/s within 0–0.5 s and then moves at a constant speed. Within this time period, the driving torque fluctuates in a small range, with a peak value of 28 N m. Within 3–5 s, the robot switches from the minimum radius state to the maximum radius state, and the driving torque fluctuation increases during this time period, with a peak value of 55 N m. The centroid velocity increases. Within 5–7 s, the robot moves at a constant speed, and the driving torque fluctuates smoothly, with a maximum value of 23 N m. The centroid velocity changes periodically between 0.67 m/s and 0.8 m/s. Within 7–9 s, the robot is in the process of obstacle surmounting, and the height of the centroid increases. During this

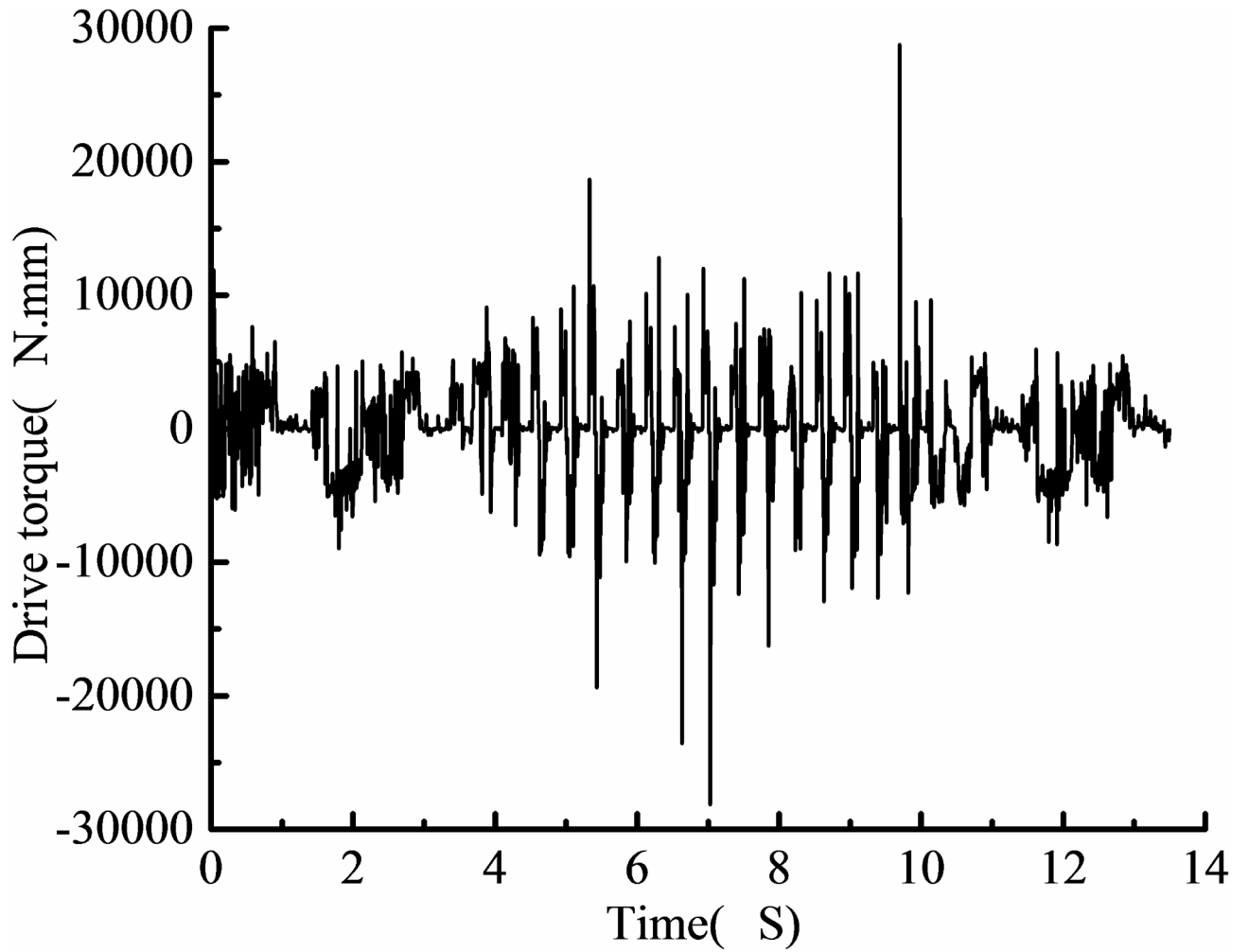


Fig. 8. Drive Torque Change.

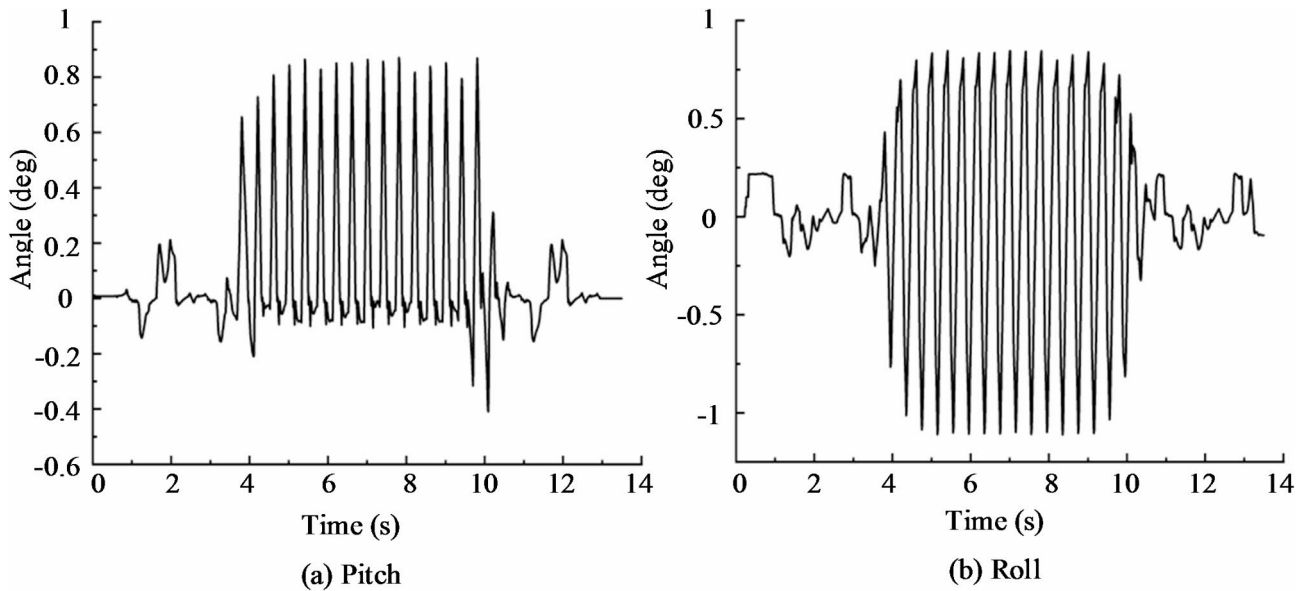


Fig. 9. Attitude angle of robot in deformation process.

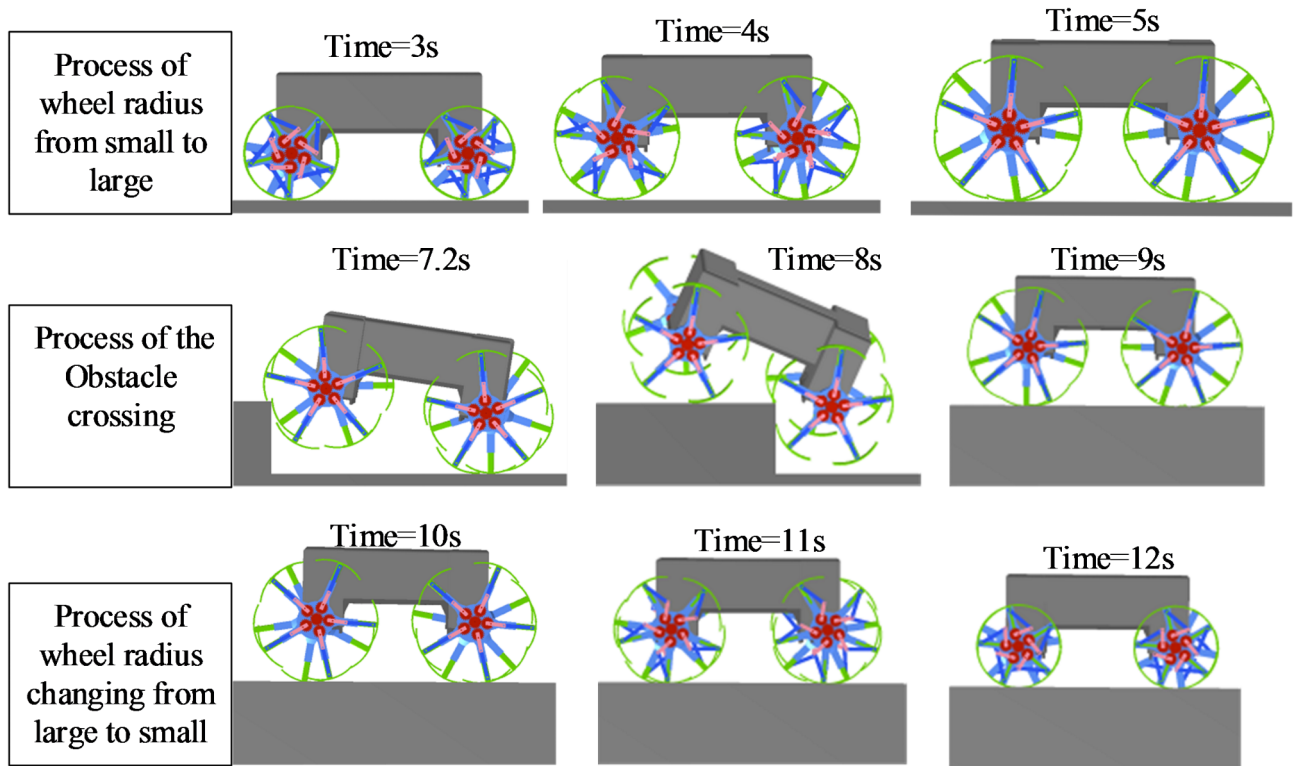


Fig. 10. Schematic diagram of the obstacle surmounting process.

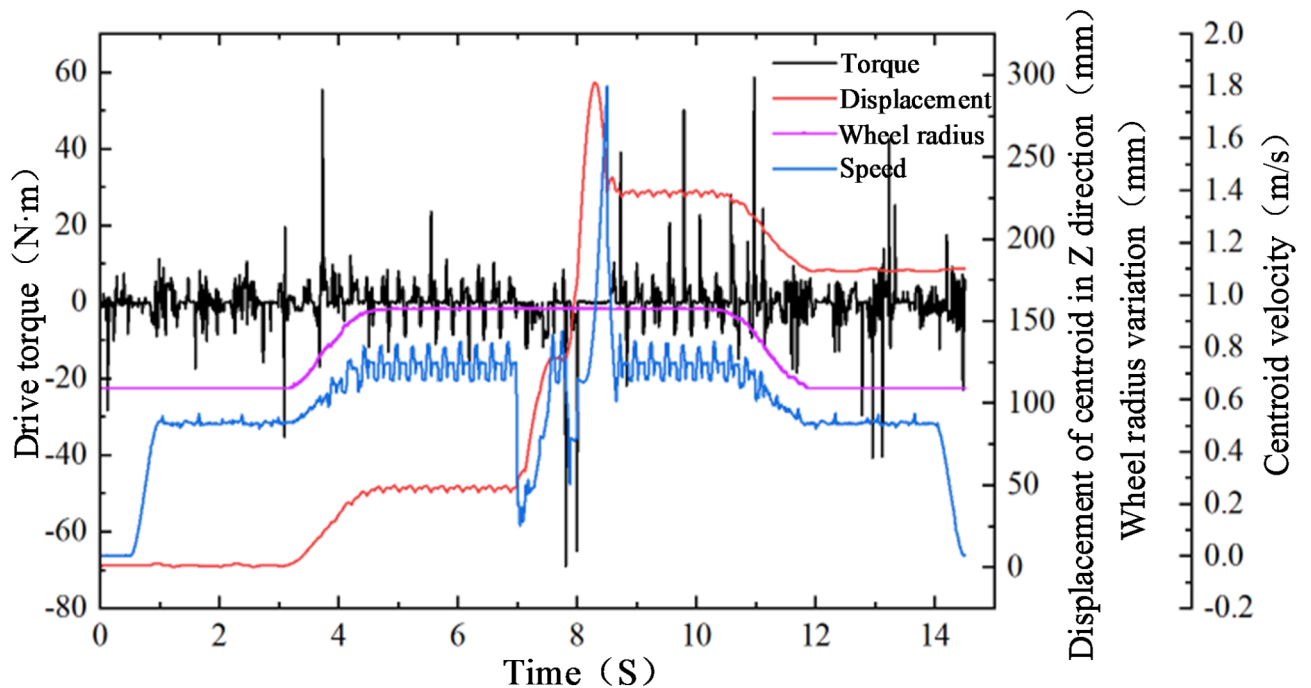


Fig. 11. Parameters of the robot obstacle surmounting process.

process, the extreme value of the driving torque is -64 N·m. Within 9–10 s, the robot keeps away from the steps with the maximum radius. Within 10–12 s, the robot switches from the maximum radius state to the minimum radius state. The robot travels with the minimum radius within 12–14 s. Within 14–14.5 s, the angular speed of the driving wheel decreases from 270 to 0 d/s. Figure 12 illustrates the posture change of the body of the robot during the obstacle surmounting process. Within 3–7 s, the wheels are deployed and the robot does not cross the

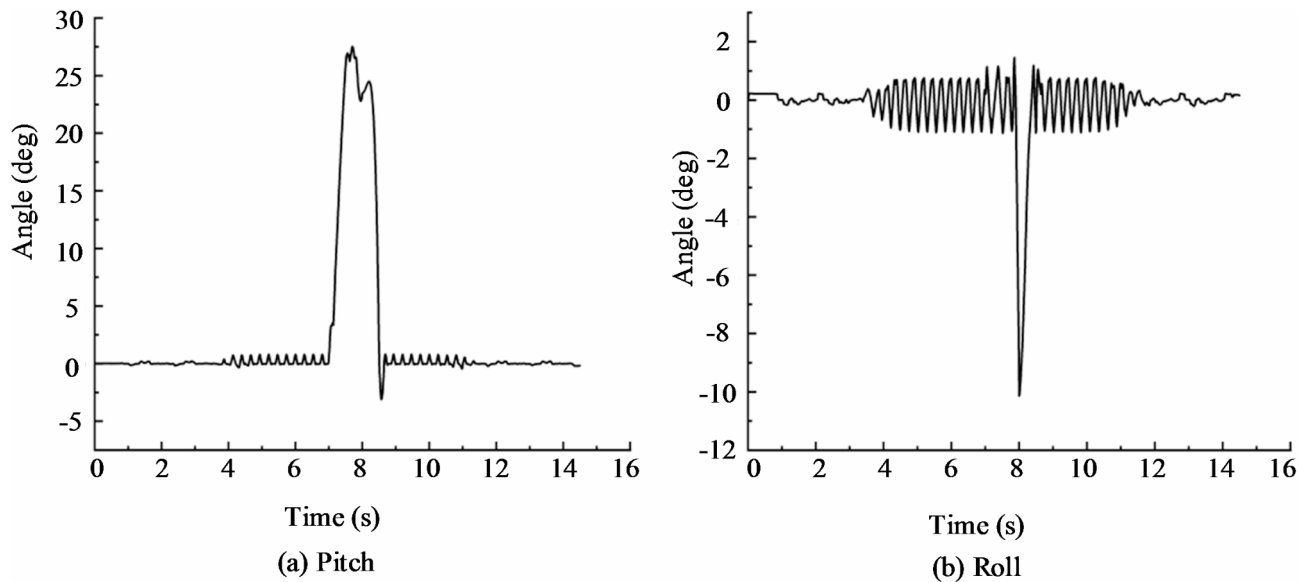


Fig. 12. Attitude angle of robot in obstacle surmounting process.

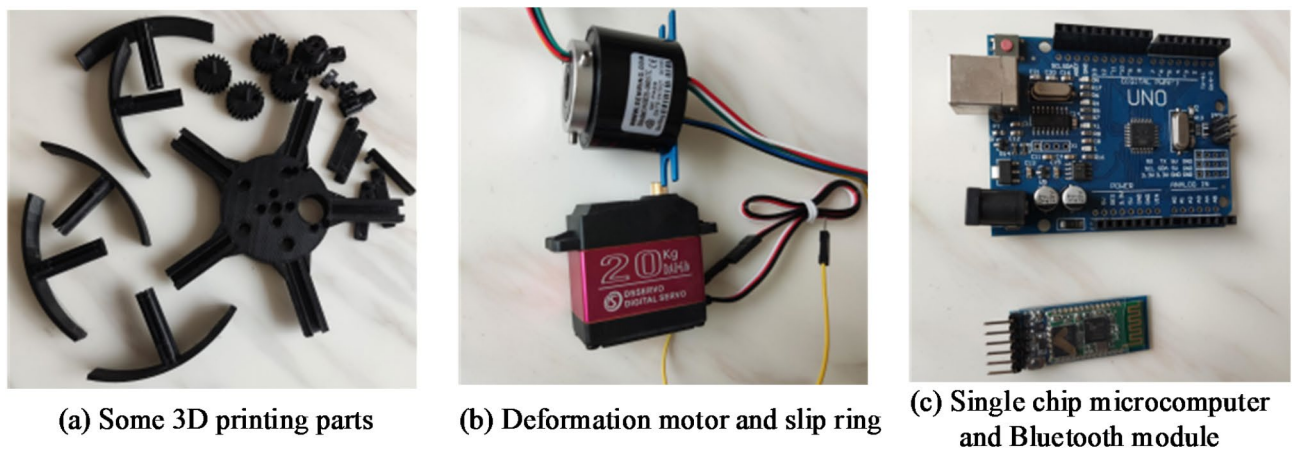


Fig. 13. Some parts.

obstacle. The posture change of the robot is the same as that of the deformation simulation. The robot starts to cross the obstacle in 7s, the front of the robot rises and lifts, the pitch angle rises to 27.5 deg, and the maximum amplitude of the roll angle is -10.2 deg. This is because the gap of the umbrella rim on one side is seized in the step during the obstacle crossing process. During the wheel driving process, the fuselage rolled along the vehicle axis, resulting in a sudden increase in the amplitude of the roll angle during the obstacle crossing process.

Experimental result

As shown in Fig. 13a, the 3D printing technology was used to print some nonstandard parts of the 3D model, including hub, gear groups, umbrella rim, connecting rod, and rocker. The deformation motor is installed on the wheel disc and connected to the vehicle body through the slip ring, as shown in Fig. 13b. An Atmega328p ch340 development board is used to control the deformation motor and drive motor. The Hc-05 Bluetooth module is selected for wireless transmission to communicate with the upper computer, as shown in Fig. 13c. $6 \times 10 \times 3$ mm and $20 \times 25 \times 4$ mm bearings are used to ensure the connection between the gear and the disc, as shown in Fig. 14a. High strength chrome-plated steel with a diameter of 8 mm is selected as the axle. The axle is connected to the wheel disc through a flange, the axle is connected to the vehicle body through a KP08-type vertical seat bearing, and the axle is connected to the drive motor through a 4×8 mm universal joint, as shown in Fig. 14b,c.

Based on the gear connecting rod slider mechanism, the solid model of the developed variable diameter wheel is shown in Fig. 15a, the module composed of a group of wheels and the driving motor is shown in Fig. 15b, and the prototype of the robot is shown in Fig. 15c. According to the simulation test results, under the condition that the robot battery is fully charged, the heights of the outdoor ground obstacles are set as 188 mm,

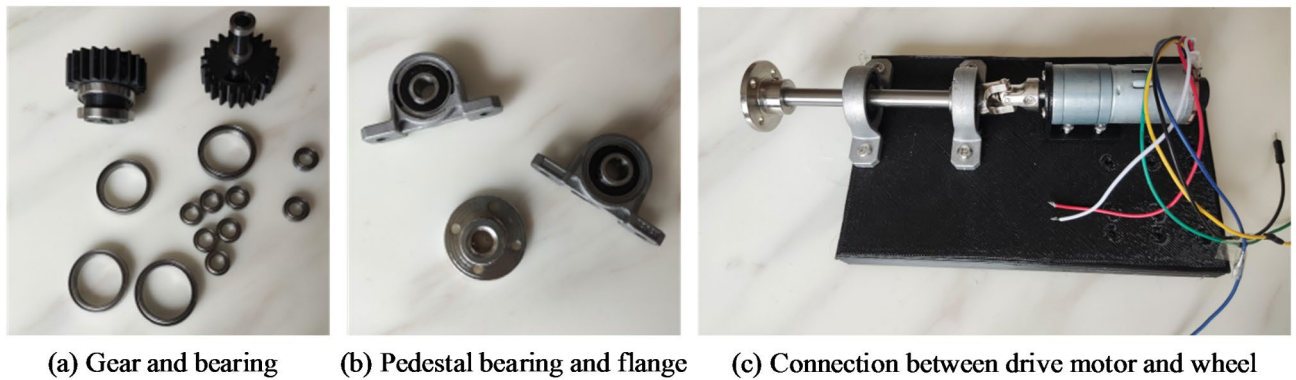


Fig. 14. Transmission relations.

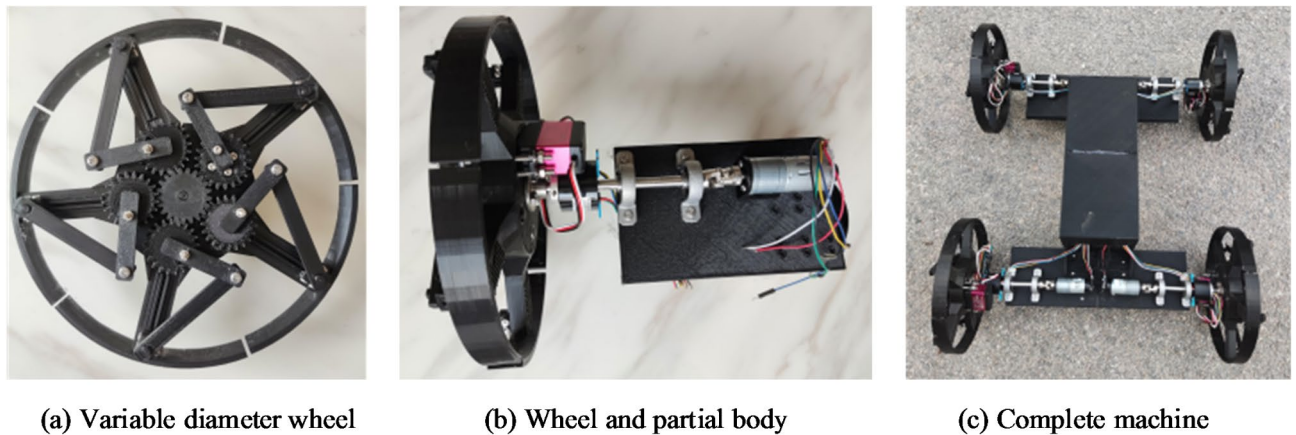


Fig. 15. Robot prototype.

184 mm, 180 mm, 176 mm, 172 mm and 168 mm. The prototype test verifies that the robot successfully climbed 172 mm obstacles and failed to climb 176 mm obstacles. Through fine adjustment of the obstacle height from 172 to 176 mm, the limit obstacle crossing height of the robot was finally determined to be 172 mm, the turning radius is 11.6 mm. The obstacle crossing process of the robot is shown in Fig. 16, and the obstacle crossing height is shown in Fig. 17. The attitude angle of obstacle crossing experiment is shown in Fig. 18.

It can be seen from Fig. 17 that the actual maximum obstacle crossing height of the robot is 172 mm, and the error between the simulation test and the prototype test is 4.4%. The error may be caused by the gear meshing clearance and the slide rail clearance. Moreover, the wheels driven by the simulation are infinitely powered and have no power consumption limitation. In the actual test, it is also related to the battery power and motor torque. It can be seen from Fig. 18 that the shape of the attitude angle image is basically the same as that of the simulation during the experiment, and the fluctuation of the experimental data is much smoother than that of the simulation. This is because the robot is made of 3D printing and is made of plastic material with weak rigidity, low accuracy and large gap, which has a certain buffer effect on the impact. As shown in Fig. 18a, the pitch angle of the robot obtained from the experiment does not drop to a negative angle when it is about to cross the steps. This is due to the speed drive added by the simulation, the infinite power, and the rear wheel elevates the rear of the robot when it crosses the steps, so the rear of the robot is higher than the front in a short time. As shown in Fig. 18b, the roll angle obtained by the experiment is larger than that obtained by the simulation test because the power consumption of the experimental prototype is limited. The two rear wheels do not cross the steps synchronously during the obstacle crossing process, resulting in a side-tilt of the body. Based on the above simulation and experimental results, compared with existing coal mine robots^{35–37}, the obstacle crossing height of the robot designed in this paper will be increased by 60.7% after the wheels are unfolded, while the track wheel leg deformation in reference³⁶ only increases by 16.7%. Moreover, the robot designed in this paper has high flexibility and light weight, and can accelerate forward by freely contracting the wheel diameter. When encountering obstacles, the wheels will be unfolded to improve the obstacle crossing performance. In the future, wear-resistant rubber will be pasted on the outer edge of the wheel to further improve the posture stability of the robot.



Fig. 16. Obstacle surmounting process of robot.

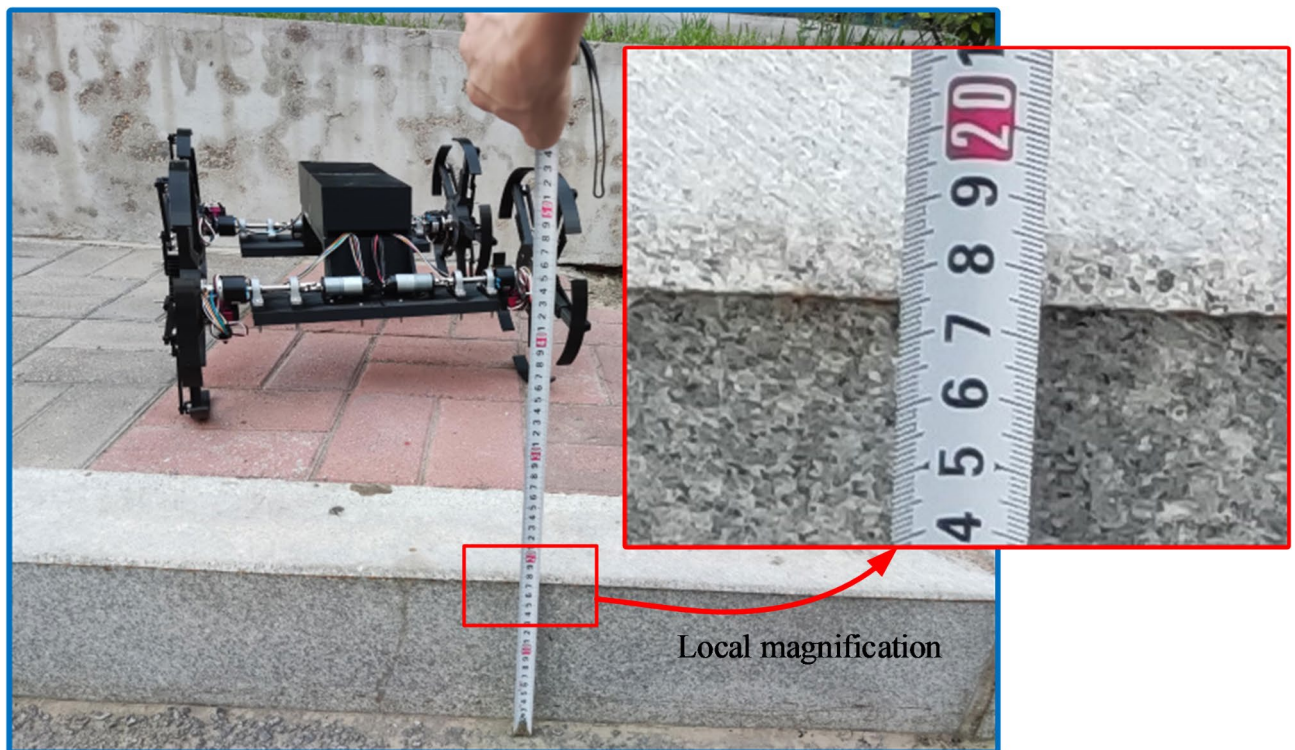


Fig. 17. Obstacle crossing height of robot.

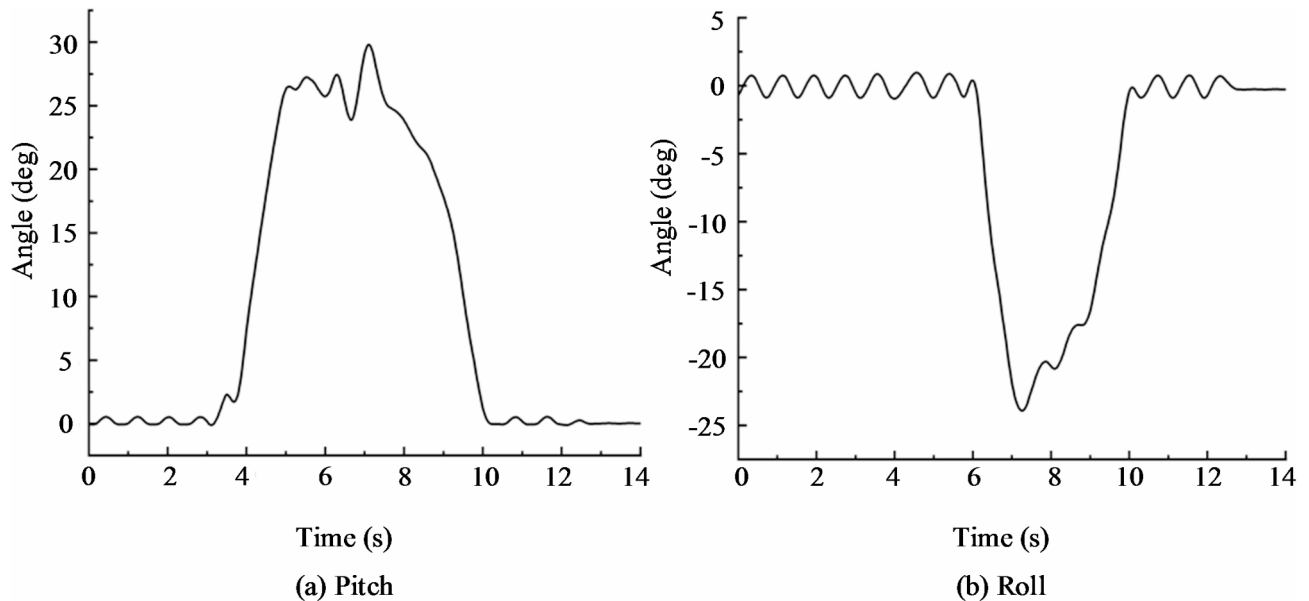


Fig. 18. Attitude angle of obstacle crossing experiment.

Conclusions

This paper creatively proposes a kind of coal mine robot with variable wheel diameter, which effectively solves the problem of coal mine robot with large volume and weak obstacle surmounting ability, which is difficult to detect in the underground unstructured environment. Through the software RecurDyn v9r4, the virtual prototype simulation test of the designed robot was carried out, and the robot prototype was made and verified. The robot keeps the minimum diameter and walks in the form of round wheels in smooth road conditions. When encountering obstacles, the wheel diameter increases and the gap between adjacent spokes can easily cross the obstacles. The diameter of the wheel is changed by a simple gear slide mechanism, and the gear is selected with appropriate standard parts. The production cost is extremely low, and the simple structure improves the reliability. The minimum radius of the variable diameter wheel is 107 mm, and the maximum radius is 158 mm. The radius of the gear connecting rod slider mechanism increased by 47.6%. The ultimate obstacle-crossing height of the robot under the maximum radius is 172 mm, which is 60.7% higher than the ultimate obstacle-crossing height of the ordinary wheeled robot. The prototype made by 3D printing technology has lower accuracy compared with the actual coal mine robot manufacturing, and the deformation motor is not in the center of the wheel, so the wheel cannot maintain dynamic balance. In the future, the steel material prototype will be manufactured in the factory, and the dynamic balance of the wheel can be ensured by installing the dynamic balance block on the wheel or improving the deformation driving mode, and the position and attitude detection and autonomous navigation functions will be built, and industrial tests will be conducted in the underground.

Data availability

All data generated or analysed during this study are included in this published article.

Received: 8 September 2024; Accepted: 5 February 2025

Published online: 22 February 2025

References

- Song, J. Development and application of dangerous gas inspection robot in coal mine. *J. Intell. Mine* **3** (01), 50–53 (2022).
- Ma, X. Research on inspection robot in coal mine. *J. Coal Technol.* **40** (10), 169–172. <https://doi.org/10.13301/j.cnki.ct.2021.10.041> (2021).
- Zhu, H. & You, S. Research and experiment of a new type of coal mine rescue robot. *J. China Coal Soc.* **45** (6), 2170–2181. <https://doi.org/10.13225/j.cnki.jccs.ZN20.0352> (2020).
- Yang, C. & Zhang, X. A review: Key technologies of coal mine robots for environment perception and path planning. *J. China Coal Soc.* <https://doi.org/10.13225/j.cnki.jccs.2021.1130> (2021).
- Lee, D., Kim, S., Kim, J., Park, J. & Cho, K. Origami wheel transformer: A variable-diameter wheel drive robot using an origami structure. *J. Soft Rob.* **4** (2), 163–180. <https://doi.org/10.1089/soro.2016.0038> (2017).
- Nagatani, K., Kuze, M. & Yoshida, K. Development of transformable mobile robot with mechanism of variable wheel diameter. *J. Robot Mechatron.* **19**, 252–253. <https://doi.org/10.20965/jrm.2007.p0252> (2007).
- Chen, X., Gao, F., Yao, S. & Wang, Z. Principle and dynamics simulation analysis of varying strategy of a novel variable diameter walking wheel. *J. Adv. Mater. Res.* **308–310**, 1875–1879. <https://doi.org/10.4028/www.scientific.net/AMR.308-310.1875> (2011).
- Koh, J., Lee, D., Kim, S. & Cho, K. Deformable soft Wheel Robot using hybrid actuation. in *Intelligent Robots and Systems (IROS), 2012 IEEE/RSJ International Conference on IEEE* 3869–3870. <https://doi.org/10.1109/IROS.2012.6386291> (2012).
- Koh, J., Lee, D. & Cho, K. Design of the shape memory alloy coil spring actuator for the soft deformable wheel robot. in *International Conference on Ubiquitous Robots & Ambient Intelligence IEEE* 641–642 <https://doi.org/10.1109/URAI.2012.6463107> (2012).

10. Zhao, X., Su, W. & Zhang, S. The simulation and analysis of a new rescue robot with transformable wheels. in *World Conference on Mechanical Engineering and Intelligent Manufacturing* 545–548. <https://doi.org/10.1109/WCMEIM48965.2019.00116> (2019).
11. Guo, P. Research and design of the deformation wheel adapting to Complex conditions. *J. Mach. Des.* **32** (07), 41–46. <https://doi.org/10.13841/j.cnki.jxsj.2015.07.009> (2015).
12. Xie, X. & Gao, F. Tractive performance analysis of transformable wheel on soft terrain. *J. Trans. Chin. Soc. Agric. Mach.* **47** (s1), 457–463. <https://doi.org/10.6041/j.issn.1000-1298.2016.S0.069> (2016).
13. Yang, Y., Zhang, Z., Guang, H. & Wang, Y. A Kind of multistage transformable wheel for mobile robots. *J. Beijing Univ. Aeronaut. Astronaut.* **44** (8), 1712–1719. <https://doi.org/10.13700/j.bb.1001-5965.2017.0580> (2018). (in Chinese).
14. Cong, P., Liu, J. & Feng, X. Mechanism design and simulation analysis of deformable wheeled mobile robot. *J. J. Mech. Transmission* **45** (08), 76–83. <https://doi.org/10.16578/j.issn.1004.2539.2021.08.011> (2021).
15. Deng, Z., Yu, B. & Ceng, S. Design and motion analysis of a deformable wheel with heavy load. *J. Mod. Manuf. Technol. And* **58** (03), 14–16. <https://doi.org/10.16107/j.cnki.mmte.2022.0201> (2022).
16. Chan, Z. et al. Motion drive and multi-mode control method of an electric parallel six wheel-legged robot. *J. Robot* **42** (5), 534–549. <https://doi.org/10.13973/j.cnki.robot.190524> (2020).
17. Chen, Z. et al. Control strategy of stable walking for a hexapod wheel-legged robot. *J. ISA Trans.* **108** (3), 367–380. <https://doi.org/10.1016/j.isatra.2020.08.033> (2020).
18. Chen, Z., Li, J., Wang, S., Wang, J. & Ma, L. Flexible gait transition for six wheel-legged robot with unstructured terrains. *J. Rob. Auton. Syst.* **150** (103989), 1–18 (2022).
19. Shang, Z., Zhao, L., Liu, X. & Jin, X. Deployable Waterbomb Wheel structure analysis and optimization of Mine Rescue Robots. *J. China Mech. Eng.* **32** (24), 2924–2933. <https://doi.org/10.3969/j.issn.1004-132X.2021.24.004> (2021).
20. Liu, X. *Research on Design of Coal Mine Rescue Robot with Variable Wheel Diameter* (Liaoning University of Engineering and Technology, 2021). <https://doi.org/10.27210/d.cnki.glnju.2021.000248>
21. Shang, Z. *The Design and Properties Research of the Foldable Waterbomb Wheel Structure of the Coal Mine Rescue Robot* (Liaoning University of Engineering and Technology, 2021). <https://doi.org/10.27210/d.cnki.glnju.2021.000014>
22. Zhao, L. et al. Analysis of mechanical behaviors of waterbomb thin-shell structures under quasi-static load. *J. AIP Adv.* **11** (5), 055215. <https://doi.org/10.1063/5.0050396> (2021).
23. Rubio, F., Valero, F. & Llopis-Albert, C. A review of mobile robots: Concepts, methods, theoretical Framework, and applications. *J. Int. J. Adv. Robotic Syst.* **16** (2), 172988141983959. <https://doi.org/10.1177/1729881419839596> (2019).
24. Zhang, A., Huo, D. & Li, D. Design of towed Inspection robot for fully mechanized coal mining face. *J. Autom. Appl.* **07**, 133–135. <https://doi.org/10.19769/j.zdhy.2021.07.044> (2021).
25. Wang, L. & Chang, Z. Application and development trend of robot technology in coal mine. *J. Coal Technol.* **40** (04), 151–153. <https://doi.org/10.13301/j.cnki.ct.2021.04.045> (2021).
26. Song, Y., Zheng, Y., Liu, Y., Ma, X. & Li, Y. Analysis on the application and prospect of coal mine bionic robotics. *J. China Coal Soc.* **45** (06), 2155–2169. <https://doi.org/10.13225/j.cnki.jccs.zn20.0328> (2020).
27. Zhang, F. Design of variable diameter detection robot for colliery pipes. *J. Min. Process. Equip.* **39** (08), 116–119. <https://doi.org/10.16816/j.cnki.ksjx.2011.08.033> (2011).
28. Ge, S., Hu, E. & Pei, W. Classification system and key technology of coal mine robot. *J. China Coal Soc.* **45** (01), 455–463. <https://doi.org/10.13225/j.cnki.jccs.YG19.1478> (2020).
29. Chen, Y., Huo, Z., Liu, Z. & Zhang, Y. Development trend and key technology of coal mine transportation robot in China. *J. Coal Sci. Technol.* **48** (07), 233–242. <https://doi.org/10.13199/j.cnki.cst.2020.07.024> (2020).
30. Yang, D. *Research and System Design of Deformable Walking Mechanism of Rescue Robot* (Liaoning University of Engineering and Technology, 2020). <https://doi.org/10.27210/d.cnki.glnju.2020.000212>
31. Zhao, X. *Design and Simulation of Search and Rescue Robot with Transformable Wheel* (Military Academy of Sciences, 2020). <https://doi.org/10.27193/d.cnki.gjsky.2020.000040>.
32. Zhang, P. *Design and Analysis of Perceptible Variable-spoke Wheel for Manned Lunar Rover* Chongqing University, 2017).
33. Zhao, L., Zhang, H., Yue, H. & Chen, Y. Path and trajectory of manipulator in laser cladding of shearer blade. *J. China Coal Soc.* **45** (S2), 1041–1051. <https://doi.org/10.13225/j.cnki.jccs.2020.0167> (2020).
34. Jia, B., Mao, S., Chen, Y., Yu, X. & Yang, Q. Improved geometry control for SLMM-based segmental precast bridges. *J. J. Harbin Eng. Univ.* **05**, 1–8. <https://doi.org/10.11990/jheu.202010052> (2022).
35. Yong, J. Mechanical structure design of coal mine detection robot. in *IOP Conference Series: Earth and Environmental Science* vol. 170(2) (IOP Publishing, 2018) p 022138.
36. Shang, L., Wang, H., Si, H., Li, Y. & Pan, T. Investigating the obstacle climbing ability of a coal mine search-and-rescue robot with a hydraulic mechanism. *J. Appl. Sci.* **12** (20), 10485 (2022).
37. Wang, W., Dong, W., Su, Y., Wu, D. & Du, Z. Development of search-and-rescue robots for underground coal mine applications. *J. Field Rob.* **31** (3), 386–407 (2014).

Author contributions

L.H. provided materials, laboratory tools and facilities. F.D.,L.Z. planned and supervised the study. L.H.,M.L. assisted with the model analysis and results. P.L.,C.L. ,L.L.carried out the simulation model construction, the implementation of the experiment, experimental data analysis, image graphics, manuscript writing and preparation. M.L.,L.R.,Y.L. assisted with the literature survey. All authors read and commented on the manuscript.

Funding

This work was supported by the Open Fund of Anhui Engineering Research Center for Intelligent Computing and Information Innovation [Grant number ICII202406] and the Fuyang Normal University Doctoral Research Initiation Fund [Grant number 2023KYQD0048].

Declarations

Competing interests

The authors declare no competing interests.

Additional information

Correspondence and requests for materials should be addressed to F.D.

Reprints and permissions information is available at www.nature.com/reprints.

Publisher's note Springer Nature remains neutral with regard to jurisdictional claims in published maps and institutional affiliations.

Open Access This article is licensed under a Creative Commons Attribution-NonCommercial-NoDerivatives 4.0 International License, which permits any non-commercial use, sharing, distribution and reproduction in any medium or format, as long as you give appropriate credit to the original author(s) and the source, provide a link to the Creative Commons licence, and indicate if you modified the licensed material. You do not have permission under this licence to share adapted material derived from this article or parts of it. The images or other third party material in this article are included in the article's Creative Commons licence, unless indicated otherwise in a credit line to the material. If material is not included in the article's Creative Commons licence and your intended use is not permitted by statutory regulation or exceeds the permitted use, you will need to obtain permission directly from the copyright holder. To view a copy of this licence, visit <http://creativecommons.org/licenses/by-nc-nd/4.0/>.

© The Author(s) 2025